Filtration Gas Combustion in a Porous Ceramic Annular Burner for Thermoelectric Power Conversion

Bubnovich V. I.* San Martin P.I. and Henriquez L.
Department of Chemical Engineering,
Universidad de Santiago de Chile,
Chile,
E-mail: valeri.bubnovich@usach.cl

ABSTRACT

A numerical study of the combustion of lean methane/air mixtures in a porous media burner is performed using a novelty geometry, cylindrical annular space. The combustion process takes place in the porous annular space located between two pipes, which are filled with alumina beads of 5.6 *mm* diameter (Al_2O_3) forming a porosity of 0.4. The outer tube diameter of 3.82 *cm* is isolated; meanwhile the inner tube of 2 *cm* in diameter is covered by a continuous set of thermoelectric elements (*TEE*) for transforming heat energy into electricity. To achieve and maintain the proper temperature gradient on *TEE*, convective heat losses are considered from the *TEE*. The respective heat transfer coefficient is variable and is in the range $800 < h < 1500$ [W / m^2]. The *2D* mathematical model includes the energy equations for solid and gas phases, the momentum equations, the continuity equation, the fuel mass conservation, the perfect gas law and it is solved by Means of computational simulations in *COMSOL Multiphysics*. Computer simulations focus on the two-dimensional temperature analysis and displacement dynamics of the combustion front inside the reactor, depending on the values of the filtration velocity ($0.1 < u_{g0} < 1.0$, *m/s*) and the fuel equivalence ratio ($0.06 < \Phi < 0.5$). The conditions that maximized the overall performance of the process of energy conversion are $u_{g0} = 0.7$ [*m / s*], $\Phi = 0.363$ and $h = 1500$ [W/m^2K], to obtain 2.05 [*V*] electrical potential, 21 [*W*] of electrical power and an overall efficiency of process $\eta = 5.64\%$. The study shows that the cylindrical annular geometry can be used for converting the energy of combustion from lean gas mixtures into electricity, with a performance similar to the specified by manufacturers of TEEs.

INTRODUCTION

The need to lower emissions and increase efficiency in fossil fuel combustion has driven the search of new combustion methods and advanced burner designs. A porous media burner can provide a good solution due to a number of advantages compared to conventional free-flame combustion, such as large power variation range, high efficiency, compact structure with very high energy concentration per unit volume, extremely low *CO* and NO_x emissions over a wide range of thermal loads, stable combustion over a wide range of equivalence ratios, $0.4 < \Phi < 0.9$ [1–3]. All the arguments mentioned above have driven the current development of these kinds of burners, which have already found several important industrial applications [4–7]. The problem of gas combustion in inert porous media has been studied intensively both theoretically and experimentally. The most important results of both research methodologies have been summarized in [8, 9].

NOMENCLATURE

A	[s^{-1}]	Frequency factor
c	[mol/m^3]	Molar concentration
C_p	[J/kg/K]	Specific heat capacity
D	[m^2/s]	Combined diffusion coefficient
D_d	[m^2/s]	Dispersion diffusivity
D_g	[m^2/s]	Difussion coefficient
D_p	[m^2/s]	Parallel $\mathbf{D_d}$ component
D_t	[m^2/s]	Transverse $\mathbf{D_d}$ component
d_p	[m]	Particle diameter
Δh_m	[J/mol]	Molar reaction heat
E_a	[J/mol]	Activation energy
e_{ign}	[m]	Length of ignition zone
e_{wall}	[m]	Thickness of internal cylinder
e_m	[-]	Emissivity
$\boldsymbol{k}$	[W/m/K]	Effective thermal conductivity
F_c	[-]	Contact factor
h	[$W/K/m^2$]	Convective heat transfer coefficient
Pr	[-]	Prandtl number
R	[J/mol/K]	Universal gas constant
$R_{1,2,3}$	[m]	Radius in geometrical position 1, 2 or 3
Re	[-]	Reynolds Number
Y_F	[-]	Fuel mass fraction
Z_{downs}	[m]	Length of downstream zone
Z_{ign}	[m]	Length of upstream zone

Subscripts

0	Initial condition
eff	Effective expression
FC	Combustion front
g	Relative to gas phase
s	Relative to solid phase
w	Relative to cylinder walls
f	Fuel

Greek Symbols

α_{vol}	[$W/m^3/K$]	Volumetric heat transfer coefficient
ε	[-]	Porosity
μ	[kg/m/s]	Dynamic viscosity
Φ	[-]	Fuel equivalence ratio
σ	[$W/m^2/K^4$]	Stefan-Boltzmann constant

One of the most important problems of porous media burners is stabilizing the flame in a specific zone of the inert porous media. It is also important for the static combustion front to have some predefined characteristics to be able to maximize the efficiency of the burner and minimize CO and NOx emissions [2, 3, and 5]. For this purpose, four different flame control methods have been developed. The first method

considers forming two layers of the porous media in which the modified Peclet number is less than (first layer) or greater than (second layer) 65 [1–3, 8, 10–12]. The second method considers cooling the post-combustion zone [13, 14]. The third method enables retaining the flame in a specific zone of the porous media by periodically exchanging the mixture inlet and exhausting the combustion gases [15–19]. Finally, the fourth method of flame stabilization employs a porous body with non-constant cross sectional area [20]. The motion of the combustion zone results in positive or negative enthalpy fluxes between the reacting gas and solid porous media. As a result, observed combustion temperatures can significantly differ from adiabatic predictions based on the enthalpy of the initial reactants and is controlled mainly by reaction chemistry and heat transfer mechanism. Upstream wave propagation against the gas flow results in subadiabatic combustion temperature, while downstream propagation of the wave leads to combustion in the superadiabatic regime, with much higher temperatures than the adiabatic temperature [21-23]. Superadiabatic combustion significantly extends conventional flammability limits to the region of ultralow heat content mixtures.

For an adequate burner design with a specific porous media, it is imperative to know the temperature levels reached and the travel speed of the combustion front inside the porous media according to several parameters. These parameters include the physical properties of the porous media, gas filtration speed and fuel equivalence ratio, amongst others. The main results published on this subject may be found in [8, 10, 12, 21, 23 and 24]. According to investigations, the combustion front velocity is positive (front moves downstream) in the ultra-poor ($\Phi \rightarrow 0$) mixtures and is negative in mixtures close to stoichiometric ($\Phi \rightarrow 1$) throughout the range of variation of the speed gas filtration. However, for lean mixtures, i.e., those with Φ values that lie between the two extremes mentioned above, there is normally a theoretical value of the filtration gas velocity u_g^* for which $u_{FC} = 0$. As a result, for $u_g > u_g^*$, $u_{FC} > 0$ and for $u_g < u_g^*$, $u_{FC} < 0$. Moreover, the value of u_g^* increases for higher values of Φ. However, with the increased value of Φ, the positive values of u_{FC} decrease their size and the negative values of u_{FC} grow. Exactly the same is observed with increasing pore diameter of the porous medium.

The literature review shows that the combustion in inert porous media with cylindrical annular geometry was not investigated practically. For this reason, it is interesting to ask: *What properties will the combustion of methane/air lean mixtures in burners with this type of geometry have? Will these properties be different from those of combustion in the cylindrical geometry? What kind of practical applications can be made of these burners? What would be the most appropriate method for the detention or confinement of the combustion front within the porous media?* Apparently, the selected geometry is interesting for a particular application: the inner cylinder of the annular space can be used to drive a cooling fluid, such as water, for example. Then, if the inner cylinder is covered by a layer of thermoelectric elements, it will be located between two different temperatures imposed on their opposing surfaces: on one side, the temperature of the coolant, and secondly, the surface temperature of the inner cylinder in the annulus burner.

PHYSICAL SITUATION

The burner analyzed in this work is made of two stainless steel tubes of different diameters, one placed inside the other, with its annular space filled with alumina balls, as shown in Figure 1. The external cylinder of the burner is insulated, while the interior cylinder has interfacial energy losses from the reactor to the cylindrical space in the middle of the burner where a coolant fluid circulates. This heat flow is done through a set of TEE covering the inner cylinder burner. The combustion of the lean fuel gaseous mixture takes place in the annular space filled by the porous media. The mixture is ignited in the region located at half the height of the reactor, imposing the initial ignition temperature there. As a result, combustion front moves along the reactor upstream or downstream, depending on the physical conditions assigned to four different variables: gas filtration rate, fuel equivalence ratio, heat loss from the internal cylinder of the burner and the radius of the cylinder itself. Combustion development is analyzed for each combination of these four parameters, including the combustion front velocity and the two-dimensional transient temperature profiles that are generated.

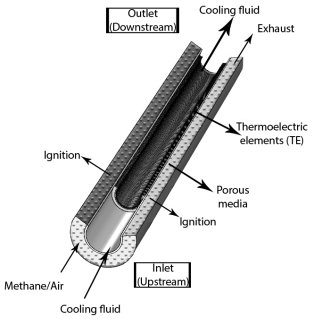

Figure 1 Burner Diagram

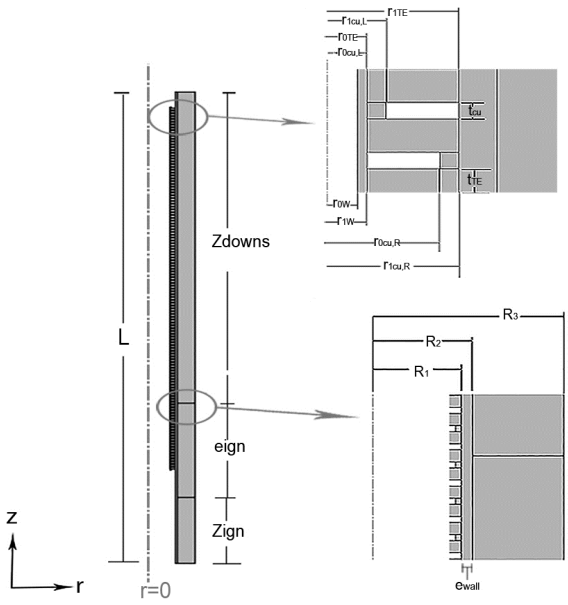

Figure 2 Burner diagram used in computer simulations

The porous media annular burner shown in Figure 1 is shown diagrammatically with its geometry in Figure 2. The system is composed of two tubes of length L and internal radius R_3 and R_1, respectively. Through the inner tube radius R_1 passes a coolant fluid, which cools a set of ETE lining the tube. This set of thermoelectric elements consists of 128 pairs of $Bi2Te_3$ p-n type semiconductors connected electrically in series and thermally in parallel, collecting the heat of chemical reaction and generating electricity.

MATHEMATICAL MODEL

The mathematical model presented below, which is made up of equations governing the combustion process of lean methane/air mixtures in porous media according to the global reaction:

$$CH_4 + 2(1+\varphi)(O_2 + 3.76N_2) \rightarrow CO_2 + 2H_2O + 2\varphi O_2 + 7.52(1+\varphi)N_2 \quad (1)$$

Where φ is the excess air coefficient of the mixture that has the following relation with the fuel equivalence ratio Φ:

$$\Phi = {}^{1}/_{(1+\varphi)} \quad (2)$$

When using a compressible fluid, the conservation of mass is given by:

$$\frac{\partial \rho_g}{\partial t} + \nabla \cdot (\rho_g \boldsymbol{u_g}) = 0 \quad (3)$$

Where $\boldsymbol{u_g}$ represents the gas filtration velocity and gas density ρ_g is governed by the ideal gas law:

$$\rho_g = \frac{pM_g}{RT_g} \quad (4)$$

Where T_g is the temperature of the gas phase and M_g is the molar mass of the mixture that is a function of Φ.

The equation of fuel mass conservation, considering single step kinetics is given by:

$$\frac{\partial c}{\partial t} + \boldsymbol{u_g} \cdot \nabla c = \nabla \cdot (D\,\nabla c) - Ace^{\frac{-E_a}{RTg}} \quad (5)$$

Where c is the methane concentration in mol/m^3, $A = 2.6 \cdot 10^8$ *[1/s]* is the frequency factor, $E_a = 1.3 \cdot 10^5$ *[J/mol]* is the activation energy and $\boldsymbol{D}$ is the effective diffusion tensor of the mixture in m^2/s, which considers both, the contribution by molecular diffusion (D_g) and dispersion ($\boldsymbol{D_d}$) [23]:

$$\boldsymbol{D} = D_g \mathbf{I} + \boldsymbol{D}_d \quad (6)$$

The dispersion tensor coefficient is given by:

$$\boldsymbol{D_d} = \begin{bmatrix} D_p{\tau_z}^2 + D_t{\tau_z}^2 & (D_p - D_t)\tau_z\tau_r \\ (D_p - D_t)\tau_z\tau_r & D_p{\tau_z}^2 + D_t{\tau_z}^2 \end{bmatrix} \quad (7)$$

Where τ_z and τ_r represent the normalized axial and radial components of the velocity vector:

$$\tau = \frac{\boldsymbol{u_g}}{|\boldsymbol{u_g}|} \quad (8)$$

The parallel D_p and transversal D_t components of the dispersion tensor $\boldsymbol{D_d}$ are defined [1] as:

$$D_p = 0.5 d_p |\boldsymbol{u_g}| \quad (9)$$

$$D_t = 0.1 d_p |\boldsymbol{u_g}| \quad (10)$$

Where d_p is the pore diameter.

The energy conservation equation for the fluid phase is expressed as:

$$\rho_g Cp_g \frac{\partial T_g}{\partial t} + \rho Cp_g \boldsymbol{u_g} \nabla T_g = \nabla \cdot (\boldsymbol{k} \cdot \nabla T_g) + Ace^{\frac{-E_a}{RT_g}} \cdot \Delta h_m - \frac{\alpha_{vol}}{\varepsilon} \cdot (T_g - T_s) \quad (11)$$

Where Δh_m= 847000 *J/mol* is the molar heat of the chemical reaction and ε represents the porosity of the porous matrix. The physical properties of the fluid are approximated to air [4]:

$$\boldsymbol{k} = k_g + 0.5 \rho_g C_p \mathrm{d}_p \boldsymbol{u_g} \quad (12)$$

$$Cp_g = 947 e^{1.83 \cdot 10^{-4} T_g} \quad (13)$$

$$k_g = 4.82 \cdot 10^{-7} Cp_g T_g^{0.7} \quad (14)$$

$$\mu_g = 3.37 \cdot 10^{-7} T_g^{0.7} \quad (15)$$

Where k_g is the thermal conductivity, μ_g is the dynamic viscosity and Cp_g is the specific heat capacity of the gas phase, respectively. As noted, effective gas conductivity includes both thermal conductivity and its dispersion component. In the same equation (11) α_{vol} is the volumetric heat transfer coefficient between the solid and liquid phases [2, 3]:

$$\alpha_{vol} = \frac{6 k_g (1-\varepsilon)}{{\mathrm{d}_p}^2} (2 + 1.1 Pr^{1/3} Re^{0.6}) \quad (16)$$

Where Pr and Re are the dimensionless numbers of Prandtl and Reynolds:

$$Pr = \frac{\mu_g Cp_g}{k_g} \quad (17)$$

$$Re = \frac{\rho_g \varepsilon |\boldsymbol{u_g}| d_p}{\mu_g} \quad (18)$$

The energy conservation equation for the porous media:

$$(1-\varepsilon)\rho_s Cp_s \frac{\partial \mathrm{T_s}}{\partial \mathrm{t}} = \nabla \cdot (k_{s\,eff} \nabla T_s) + \frac{\alpha_{vol}}{\varepsilon} (T_g - T_s) \quad (19)$$

Where ρ_s= 3987 kg/m^3 is the alumina density and $k_{s\,eff}$ is the effective thermal conductivity of the porous media considering the conductive and radiative transport mechanisms, respectively, according to the Rosseland approximation [5]:

$$k_{seff} = F_C(1-\varepsilon)k_s + \frac{32\,\sigma\,d_p\,\varepsilon e_m}{9(1-\varepsilon)}T_s^3 \quad (20)$$

Where $F_C = 0.01$ is the contact factor between the alumina balls, e_m is the emissivity of the porous material and σ is the Stefan-Boltzmann constant. The physical properties of the porous matrix are also functions of the temperature [5]:

$$Cp_s = 29.567 + 2.6117T_s - 0.0017{T_s}^2 + 3.382\cdot 10^{-7}{T_s}^3 \quad (21)$$

$$k_s = -0.21844539 + 0.00174653T_s + 8.2266{T_s}^2 \quad (22)$$

The energy conservation equation for the inner tube is:

$$\rho_w Cp_w \frac{\partial \mathrm{T}w}{\partial \mathrm{t}} = \nabla\cdot(k_w \nabla T_w) \quad (23)$$

Where $\rho_{w,} Cp_w\ y\ k_w$ are the density, specific heat and thermal conductivity of the inner cylinder, respectively. Their values were considered as those of stainless steel.

Heat transfer between the inner tube of the reactor and the cooling fluid, which is at constant temperature T_{cool}, is described by the following equation:

$$\boldsymbol{q_0} = h(T_{cool} - T_w) \quad (24)$$

Where h represents the convective heat transfer coefficient and T_w, the tube surface temperature. The fluid pressure drop due to the presence of the porous media is described by Darcy's equation:

$$\boldsymbol{u_g} = -\frac{k_d}{\mu_g}\nabla p \quad (25)$$

Where the permeability of the porous media k_d is [6]:

$$k_d = \frac{d_p^2\,\varepsilon^2}{(1-\varepsilon)^2 150} \quad (26)$$

The initial conditions of the system are given by:

t=0:

$$\begin{cases} T_S|_{\substack{z\in[0,L]\\ \forall\, r}} = T_g|_{\substack{z\in[0,L]\\ \forall\, r}} = T_w|_{\substack{z\in[0,L]\\ \forall\, r}} = T_0 \quad P|_{\substack{z\in[0,L]\\ \forall\, r}} = P_0 \\ c|_{\substack{z\in[0,L]\\ r\in[R_2,R_3]}} = c_0 \qquad u_g|_{\substack{z\in[0,L]\\ \forall\, r}} = 0 \\ T_s|_{\substack{z\in[e_{ign}]\\ r\in[R_2,R_3]}} = T_{ign} \end{cases} \quad (27)$$

The boundary conditions are given by:

$\forall\, t, z = 0$:

$$u_g|_{r\in[R_2,R_3]} = (0, u_{g0}) \quad (28)$$

$\forall\, t, z = L$:

$$T_S|_{\forall\, r} = T_g|_{\forall\, r} = T_w|_{\forall\, r} = T_0 \quad (29)$$

$$\frac{\partial T_g}{\partial z}|_{\forall\, r} = \frac{\partial T_s}{\partial z}|_{\forall\, r} = \frac{\partial T_w}{\partial z}|_{\forall\, r}\frac{\partial c}{\partial z}|_{\forall\, r} = 0 \quad (30)$$

$\forall\, t, r = R_1$:

$$p|_{\forall\, r} = p_0 \quad (31)$$

$$\boldsymbol{q}|_{\forall\, z} = h_{cool}(T_{cool} - T_w) \quad (32)$$

$\forall\, t, r = R_2$:

$$u_g|_{\forall\, z} = (0{,}0) \quad (33)$$

$$\frac{\partial c}{\partial r}|_{\forall\, z} = 0 \quad (34)$$

$\forall\, z$: $$k_g\cdot\nabla T_g + k_S\cdot\nabla T_S = k_w\cdot\nabla T_w \quad (35)$$

$\forall\, t, r = R_3$:

$$u_g|_{\forall\, z} = (0{,}0) \quad (36)$$

$$\frac{\partial T_g}{\partial r}|_{\forall\, z} = \frac{\partial T_s}{\partial r}|_{\forall\, z} = \frac{\partial c}{\partial r}|_{\forall\, z} = 0 \quad (37)$$

The initial concentration value C_0 of the fuel in the mixture is given by:

$$C_0 = \frac{\rho}{(1+\frac{17.225}{\Phi})M_f} \quad (38)$$

Where M_f is the molar mass of the fuel.

VALIDATION OF NUMERICAL MODELS

The mathematical model (1) – (38) was computationally implemented using COMSOL Multiphysics *4.3ª*, where the following four Multiphysics were chosen: transport of diluted species (*chds*), heat transfer in fluids (*ht*), heat transfer in solids (*ht2*), Darcy's law (*dl*) and electrical currents (*ec*). That latter Multiphysic includes functions called thermoelectric effect, electromagnetic heat source, thermoelectric effect contour and electromagnetic heat source. Initial and boundary conditions were also entered into each of these Multiphysics for each of the differential equations, along with the physical properties of the respective involved substances: air, methane, stainless steel and alumina. All the numerical data values of the physical properties were entered into the "*Parameters*" window. The ideal gas law and different functions including natural gas and solid temperature dependent properties were entered into the "*Variables*" window. Cylindrical geometry was chosen *(r, z)* and it was assigned 10^{-6} relative repair tolerance value. "*Extra fine*" finite element mesh was chosen and time stepping was controlled by the variable step algorithm from the solver with an upper limit of 0.01 *s*. The convergence criteria for all variables were set when errors obtained were lower to a relative tolerance of 10^{-5}.

The work of Foutko et al. [23] was elected here for validation purposes. The authors of [23] simulate the combustion of lean mixtures of methane/air in a porous media made up of 5.6 *mm* diameter alumina balls in a 7.6 *mm*

diameter quartz cylinder in a superadiabatic regime, without local thermal equilibrium between the gas and the solid. For a special case, u_{g0} = 1.075 [m/s], Φ = 0.17 and the heat loss from the burner defined by the formula (22) in the same work, the gas and solid temperature profiles and the value of the combustion front velocity are taught in the same work. In this paper, it is computationally simulated the combustion of lean mixtures methane / air inside a quartz tube of 1.3 m in height and 76 mm in diameter, filled with alumina balls of 5.6 mm in diameter.

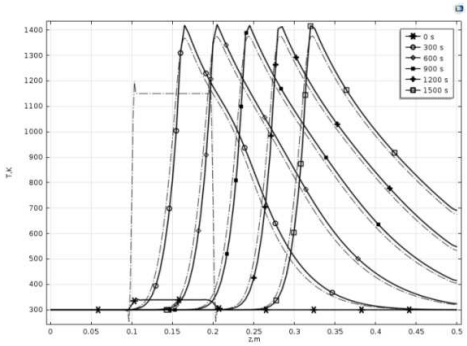

Figure 3 Combustion wave propagation: gas temperature in solid line and solid temperature in broken line, time intervals span 5 min, u_{g0} = 1.075 [m/s], Φ = 0.17.

Table 1: Physical properties of solids present in the system.

Parameter	Value	Units
Al_2O_3		
ρ_S	3987	[kg/m^3]
d_S	0.0056	[m]
Stainless steel		
cp_{ac}	440	[J/kg/K]
k_{ac}	76.2	[W/m/K]
ρ_{ac}	7870	[kg/m^3]
Copper		
cp_{cu}	385	[J/kg/K]
k_{cu}	350	[W/m/K]
ρ_{cu}	8920	[kg/m^3]
σ_{cu}	5.9·10^8	[S/m]
α_{cu}	6.5·10^{-6}	[V/K]
Ceramics		
cp_{cer}	921	[J/kg/K]
k_{cer}	27	[W/m/K]
ρ_{cer}	2350	[kg/m^3]
TEE: Bi_2Te_3		
$c_{pp} = c_{pn}$	154.4	[J/kg/K]
$k_p = k_n$	1.6	[W/m/K]
$\rho_p = \rho_n$	7740	[kg/m^3]
$\sigma_p = \sigma_n$	1.1·10^5	[S/m]
α_p	200·10^{-6}	[V/K]
α_n	-200·10^{-6}	[V/K]

The comparison between the solution [23] and this work (Figure 3) showed very similar profile temperatures. Particularly, according to [23], the highest temperature values for each phase were $T_g = 1400[K]$ and $T_S = 1350[K]$, with combustion front velocity $u_{FC} = 1.7 \cdot 10^{-4}[m/s]$, while, according to our simulations, the maximum temperatures were $T_g = 1410[K]$ and $T_S = 1356[K]$, with combustion front velocity $u_{FC} = 1.6 \cdot 10^{-4}[m/s]$. Thus, relative deviations of 0.71% were observed for the gas temperature, 0.44%, for the solid temperature and 5.9%, for the combustion front velocity.

In order to validate the correct transposition of the TEE model, Rowe and Min results presented in [25] were considered here with the intention of repeating them with the best accuracy. The main properties of different solids involved in the construction and implementation of TEE are presented in Table 1. Copper is used to bond together the elements of the hot side of the elements and ceramics is used to electrically isolate the elements of the refrigerant from the cold side. The comparison results are presented in Figure 4 where the temperature difference is the difference observed on both sides of the elements.

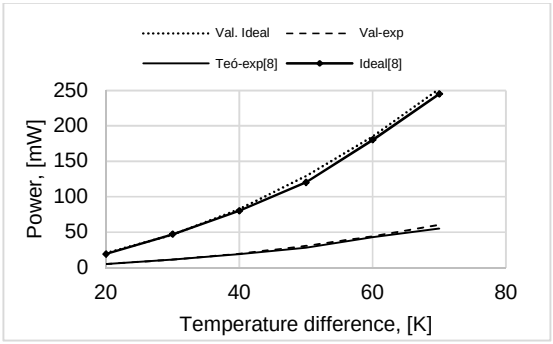

Figure 4 Electrical power obtained as a function of the temperature difference on both sides of TEE.

RESULTS

In order to analyze the two-dimensional wave propagation in a cylindrical annular space, three different parameters were varied in the work: gas filtration velocity u_{g0}, fuel equivalence ratio Φ, heat loss coefficient from the internal cylinder h and the internal cylinder radius R_1 . The variation ranges of each of the above parameters are presented in Table 2. In order to maintain laminar hydrodynamic regime in this work, the maximum value of the filtration gas velocity is limited by the value of 1 m / s.

Table 2: Values of the four variables

	Values	Units
u_{g0}	0.1, 0.3, 0.5, 0.7, 1.0	[m/s]
Φ	0.1, 0.2, 0.3, 0.4, 0.5	
h	400, 800, 1500	[$W/m^2/K$]
R_1	0.01, 0.02	[m]

For each of the four variables analyzed, we have created four different graphics representing the values of the combustion front velocity in the porous media, the temperatures along the external cylinder ($r = R_3$) and the internal cylinder ($r = R_1$ *and* $r = R_2$), and the minimum values of the fuel equivalence ratio (Φ_{min}) at which the combustion in the annular space does not extinguish (combustibility limits), depending on the gas filtrating speed. The analysis of these cases is done in the following order. First, $R_1 = 0.01\ m$ is chosen for three different values of h presented in Table 1 and the wave properties of combustion determined by u_{g0} and Φ are analyzed. Then, the same analysis is applied to the case with $R_1 = 0.02\ m$.

Figures 5 – 8 show the case of $h = 400\ W/m^2/K$. Figure 5 shows that in the five cases analyzed by Φ, for $\Phi = 0.1$, 0.2 and 0.3, the combustion wave moves downstream at a velocity whose order of magnitude is $10^{-4}\ m/s$, reaching a superadiabatic regime. In cases of $\Phi = 0.4$ and 0.5, the wave moves upstream in a subadiabatic regime. Something similar occurs with combustion wave movements in porous cylindrical media: increasing the value of Φ changes the superadiabatic regime to subadiabatic. However, a notorious change is also observed in the $u_{FC} = f(u_{g0})$ functionality for any value of Φ: the almost straight lines located absolutely above or below the horizontal axis of u_{g0} in the case of annular geometry (see figures 5, 10, 12 and 14) are changed for downward concave curves that cross axis u_{g0} at some point in circular geometry [10]. In short, for a fixed Φ, the u_{FC} combustion front velocity keeps the same sign (travel direction) regardless of the value of u_{g0}. Also, in all the cases, the combustion front velocity increases as the gas filtration velocity increases, for the same values of Φ.

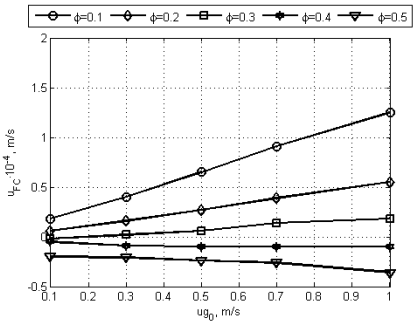

Figure 5 Combustion front velocity as function of gas entry velocity and equivalence ratio, $h_{cool} = 400\ W/m^2/K$.

Figures 6 – 8 show the maximum temperatures reached on different solid surfaces of the annular cylindrical burner: on external ($R_1 = 0.01m$) and internal ($R_2 = 0.012m$) surfaces of the internal cylinder and on the internal surface of the external cylinder ($R_3 = 0.038m$), respectively. Figure 6 shows that the highest temperatures reached on the cooled surface of the internal cylinder ($r = R_1$) is within the range of $350 < T_s < 750K$, for the analyzed values of Φ and u_{g0}. On the other hand, according to figure 7, the temperatures of the solid and the gas in $R_2 = 0.012m$ (porous media in contact with the internal surface of the same cylinder) remains within the ranges of $350 < T_s < 700K$ and $600 < T_g < 1200K$, respectively, indicating that this location does not have local thermal equilibrium: on average, $T_g - T_s \sim 400K$. For higher values of gas filtration velocity and equivalence ratio, the maximum temperatures for both gas and solid increased. Figure 8 shows that the highest temperatures of gas and solid reached in the porous media that is in contact with the insulated surface of the external cylinder of the burner is located at intervals $1100 < T_g < 1900K$ and $1050 < T_s < 1600K$, respectively. A local thermal non equilibrium in this area is also observed, where the local differences $T_g - T_s$ are in the range between 100 and 200 K, with greater differences for higher values of Φ.

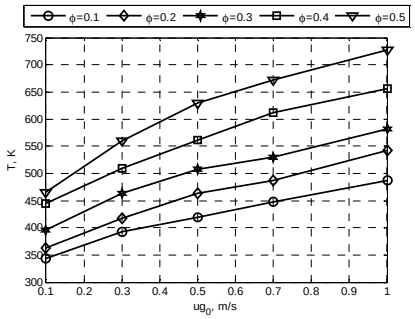

Figure 6 Solid maximum temperatures in $r = R_1$ as function of gas entry velocity and equivalence ratio, $h = 400\ W/m^2/K$.

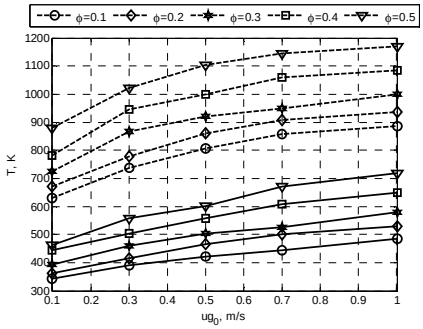

Figure 7 Maximum temperatures of gas (dotted line) and solid (solid line) in $R_2 = 0.012\ m$ as function of gas entry velocity and equivalence ratio, $h = 400\ W/m^2/K$.

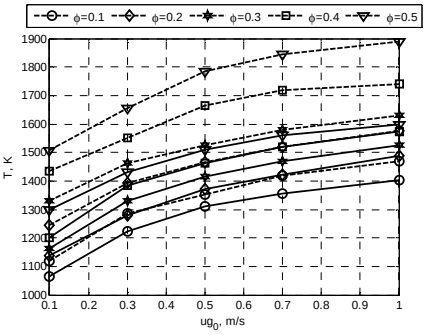

Figure 8 Maximum temperatures of gas (dotted line) and solid (solid line) in $R_3 = 0.038$ m as function of gas entry velocity and equivalence ratio, $h = 400\ W/m^2/K$.

Finally, figure 9 shows the combustibility limits according Φ_{min} values, depending on the input gas velocity $u_{g,0}$. The figure shows that these limits decrease from 0.1 up to 0.06 when the gas velocity $u_{g,0}$ increases its value from 0.1 to 1.0 *m/s*. Also, the same figure shows the highest temperatures reached by the porous media (three marked lines) and the gas (two unmarked lines) located in contact with the cooled surface of the internal cylinder (one dotted line, $r = R_1$), also on the internal surface of the same cylinder (two broken lines, $r = R_2$) and on the surface of the external cylinder (two solid lines, $r = R_3$). As seen in the figure, the temperatures of all the surfaces gradually increase with the increase of Φ. Gas temperatures of the insulated cylinder surface come near to 1500*K*, while solid temperature, on average, border 1250*K*. On the other hand, on the surface $r = R_2$, gas temperature is in the range 600 to 775*K*, showing higher values for higher Φ, while temperatures of the solid phase in the same location are around 500*K*, practically matching the temperatures of the cylinder itself, but on the cooled side, $r = R_1$ (in the figure these two lines concur).

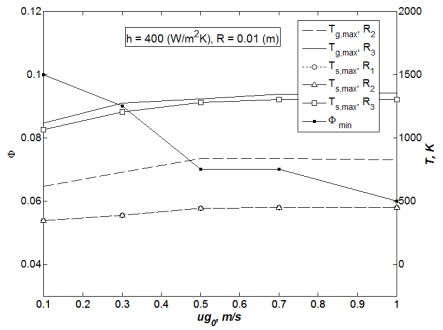

Figure 9 Combustibility limits (values of Φ_{min}) and maximum gas (dotted lines) and solid (solid lines) temperatures within the reactor in R_1, R_2 *y* R_3: R_1 = 0.01*m* and h = 400 $W/m^2/K$.

After analyzing the case with R_1 = 0.01*m* and h = 400 $W/m^2/K$, the value of h was varied, first to h = 800 $W/m^2/K$ and later to h = 1500 $W/m^2/K$, for the same value of R_1. Results showed that both the combustion front velocity and the combustibility limits of the mixture remained practically invariable, therefore the intermediate case h = 800 $W/m^2/K$ was omitted in the illustration, showing only the case with h = 1500 $W/m^2/K$ in figures 10 and 11. These figures show that the combustion front velocity, combustibility limits and temperatures of the insulated cylinder surface ($r = R_3$) did not actually suffer a noticeable change in their values. However, some changes in values of temperature are seen near the interior cylinder: both the temperatures of the gas and the solid have decreased by an average of 75°*C* on the surface $r = R_2$, just like the temperatures on the cooled surface in $r = R_1$.

Finally, the same analysis as above was repeated for the variation of $u_{g,0}$, h_{cool} and Φ, according to Table 1, but now with R_1 = 0.02 *m*. For example, comparing figure 5 with 12 and 9 with 13, respectively, the influence of the change of the inner cylinder radius R_1 can be analyzed for the same value of h = 400 $W/m^2/K$. Figures 5 and 12 show that with the increase in the value of R_1 from 0.01 to 0.02*m*, the combustion front velocity for the cases of Φ = 0.1, 0.2 and 0.3, noticeably increased their values, by up to 40% for Φ = 0.1, keeping the superadiabatic regime seen in figure 5. The figure 12 also shows that in the case Φ = 0.1, the stable combustion waves of the system only exist in the interval of gas entry velocity between 0.5 and 1.0 *m/s*. For lower values of u_{g0}, combustion does not occur and it is extinguished. On the other hand, in the subadiabatic regime with Φ = 0.4 and 0.5, the changes in the values of the combustion front velocity are much smaller, up to 10% and no qualitative changes are observed in figures 5 and 12.

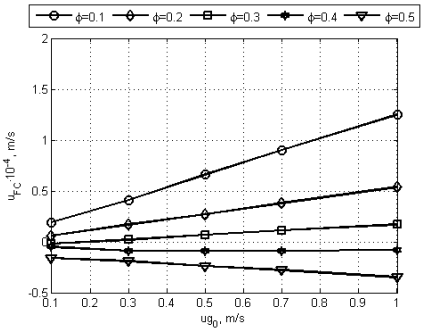

Figure 10 Combustion front velocity as function of gas entry velocity and equivalence ratio, R_1 = 0.01*m* and h = 1500 $W/m^2/K$.

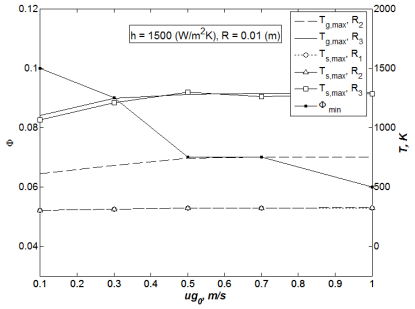

Figure 11 Combustibility limits (values of Φ_{min}) and maximum temperatures of gas (dotted lines) and solid (solid lines) within the reactor in R_1, R_2 *y* R_3: R_1 = 0.01*m* and h = 1500 $W/m^2/K$.

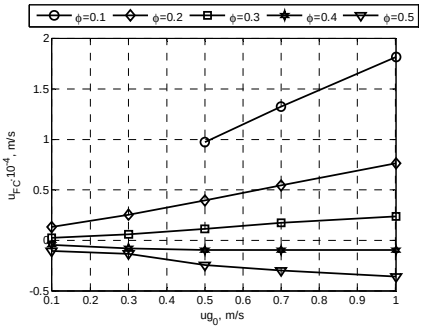

Figure 12 Combustion front velocity as function of gas entry velocity and equivalence ratio, R_1 = 0.02*m* and h_{cool} = 400 $W/m^2/K$

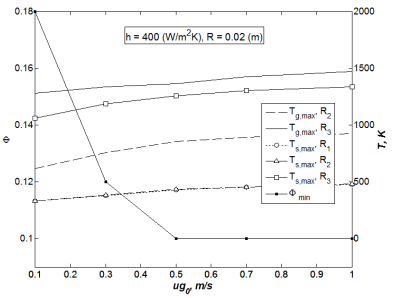

Figure 13 Combustibility limits (values of Φ_{min}) and maximum gas (dotted lines) and solid (solid lines) temperatures within the reactor at R_1, R_2 and R_3: R_1 = 0.02m and h_{cool} = 400 $W/m^2/K$.

The comparison between figures 9 and 13 shows that increasing radius R_1 from 0.01 to 0.02m significantly affects the combustibility limits of the mixture. If in the case R_1 = 0.01m the combustibility limits values are lowered from Φ_{min} = 0.1 for u_{g0} = 0.1 m/s to Φ_{min} = 0.06 for u_{g0} = 1.0 m/s, in the case R_1 = 0.02m, the same limits decrease from 0.18 to 0.1, within the same variation range of u_{g0}. Additionally, in the interval 0.5 < u_{g0} < 1.0, the values of Φ_{min} are practically the same. The same figures also show that as radius R_1 increased from 0.01 to 0.02m, the inside cylinder temperatures of the solid phase in R_1 and R_2 do not suffer major changes. Only for u_{g0} > 0.5, the temperatures in the case R_1 = 0.02m are slightly higher (~ 25°C) than in the case R_1 = 0.01m. These differences are stronger for higher values of u_{g0}. The same tendency is observed for gas temperatures in r = R_2: they have higher values in the case R_1 = 0.02m and the differences between both cases increase for higher values of u_{g0}, up to ΔT = 100°C for u_{g0} = 1.0. On the surface r = R_3, the temperatures of the porous media maintained the same values in both cases, according to the value of R_1. However, the gas temperatures of the same region, on average, were 100°C higher for the case R_1 = 0.02m.

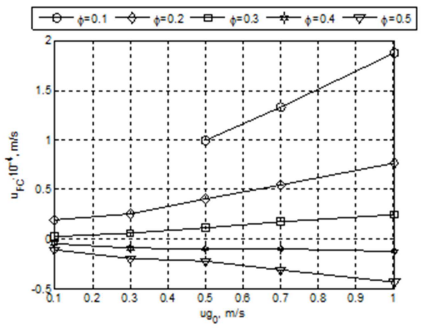

Figure 14 Combustion front velocity as function of gas entry velocity and equivalence ratio, R_1 = 0.02m and h = 1500 $W/m^2/K$.

After analyzing the case with R_1 = 0.02m and h = 400 $W/m^2/K$, the value of h was varied, first considering h = 800 $W/m^2/K$ and later, h = 1500 $W/m^2/K$, for the same value of R_1, just like in the case of R_1 = 0.01m. As a result, it was found that both combustion front velocity and combustibility limits of the mixture were practically invariable for h, therefore, only the case h = 1500 $W/m^2/K$ is presented here in figures 14 and 15, omitting the case h = 800 $W/m^2/K$. The comparison between figures 12, 13 with 14, 15 show that combustion front velocity, combustibility limits and temperatures in the cylinder surface insulated (r = R_3) have not suffered any important change in value. However, there is some decrease in values of gas temperature and the porous media near the interior cylinder (r = R_2): gas temperatures lowered by about 100°C and solids, by about 25°C.

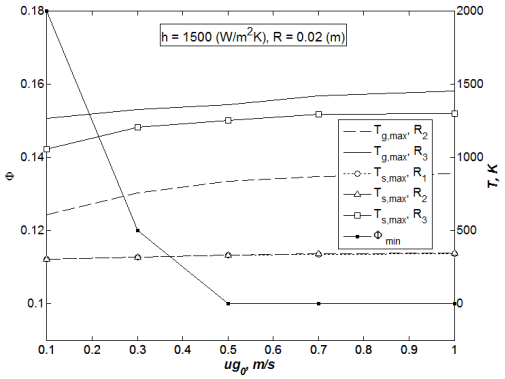

Figure 15 Combustibility limits (values of Φ_{min}) and maximum gas (dotted lines) and solid (solid lines) temperatures within the reactor at R_1, R_2 and R_3: R_1 = 0.02m and h = 1500 $W/m^2/K$.

Table3: Φ values as function of u_{g0} and h for which u_{g0} = 0: R_1 = 0.02m

	Φ		
ug_0 [m/s]	h=400 [W/(m^2·K)]	h=800 [W/(m^2·K)]	h=1500 [W/(m^2·K)]
0,1	0,3275	0,3288	0,3288
0,3	0,3388	0,3395	0,3400
0,5	0,3524	0,3327	0,353
0,7	0,3630	0,3630	0,3630
1,0	0,3750	0,3750	0,3750

As Figures 5, 10, 12 and 14 do not teach nulls of the combustion front velocity u_{FC} for different values of Φ, u_{g0} and h, computer simulations were conducted to find their values. As a result, it was found that in the case with R_1 = 0.02m, h_{cool} = 400 $W/m^2/K$ and u_{g0} = 0.1 m/s, the u_{FC} speed was null for Φ = 0.3275. Increasing u_{g0} from 0.1 to 1.0 m/s for the same value of h_{cool}, the value of Φ for which u_{FC} = 0 increases, reaching Φ = 0.375. Increasing the value of h from 400 to 1500 $W/m^2/K$ does not show considerable variations in the value of Φ for which u_{FC} = 0. A summary of these results is presented in Table 3. However, decreasing the value of R_1 from 0.02 to 0.01 m for all the values of h and u_{g0}, the values of Φ for which u_{FC} = 0 resulted lower. Particularly, in the case of u_{g0} = 0.1 m/s and h = 400 $W/m^2/K$ the result is u_{FC} = 0 when Φ = 0.276. By increasing

u_{g0} to 1.0 *m/s* the value of Φ increases and reaches 0.368. It is also noted that by varying *h* from 400 to 1500 $W/m^2/K$ for the same gas filtration velocity, the values of Φ were practically unchanged.

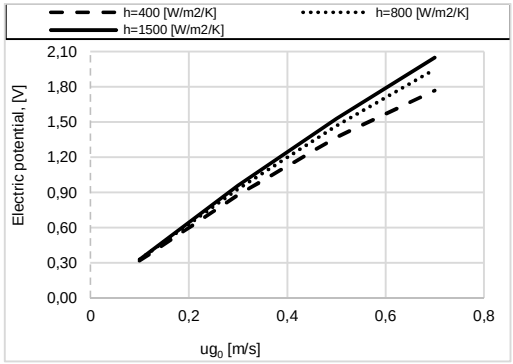

Figure 16 Electric potential produced by the TEMs.

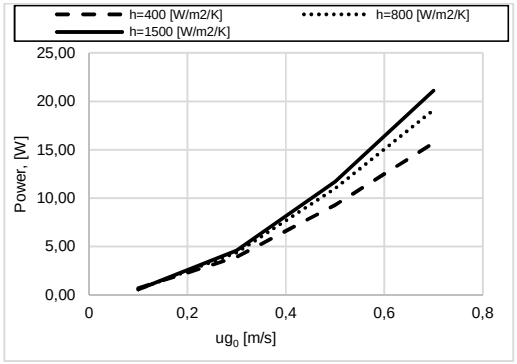

Figure 17 Electric power produced by the TEMs.

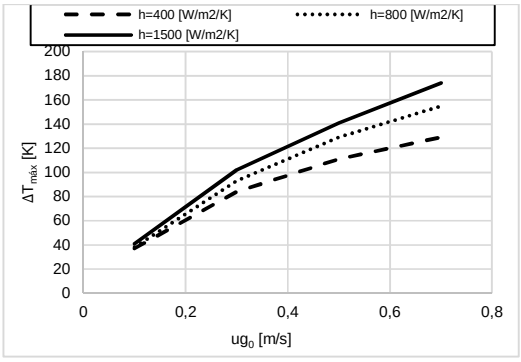

Figure 18 Temperature differences on the TEMs.

Then for all cases presented in Table 3, the electric potential, power, temperature difference, the maximum temperature and the overall efficiency of the system obtained in this work presented in Figures 16-20, respectively. From these figures it appears that with increasing both the filtration gas velocity as the convective heat transfer coefficient the electric power produced increases. The overall system efficiency was defined as the ratio of the electric energy produced and the heat released by the combustion.

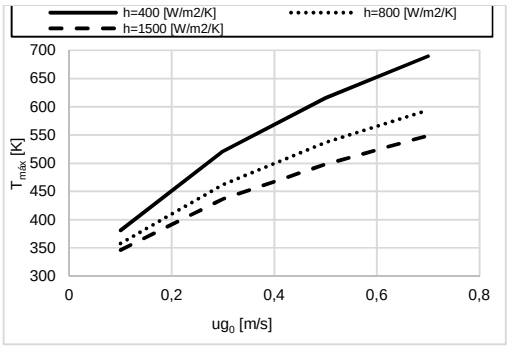

Figure 19 Maximum temperature reached on the hot side of the TEMs.

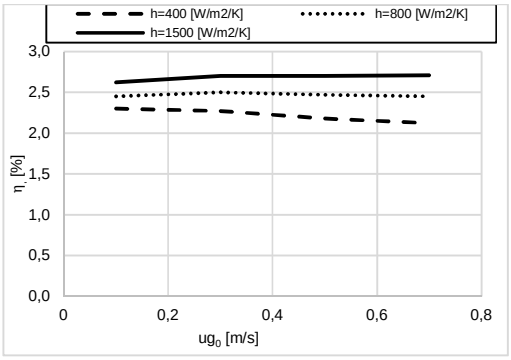

Figure 20 Overall system efficiency.

CONCLUSIONS

Computer simulations of combustion waves in annular cylindrical porous media show that, as in the case of porous cylindrical media, combustion waves are spread at a speed of around 10^{-4} *m/s*, within the variation ranges of u_{g0} and Φ considered in this work. Depending on the value of the fuel equivalence ratio Φ, these waves may move upstream, in subadiabatic regime (for greater values of Φ), or downstream, in superadiabatic regime (for lower Φ) where the thermal and combustion wave travel in the same direction (downstream) along the porous media. For the same value of Φ, when the gas filtration velocity increases, the combustion wave travels at higher speeds in the superadiabatic regime, with their values unchanged or slightly decreasing in subadiabatic regime. It is also observed that along the complete variation interval of gas entry speed $0.1 < u_{g0} < 1.0$ *m/s* the combustion front velocity has the same sign, positive or negative, if Φ is held constant. The variation of the radius in the inner cylinder noticeably affects the combustion characteristics, however, the heat loss from the inner cylinder have little effect on these, within the variation range of the considered parameters.

The conditions that maximized the overall performance of the process of energy conversion are $u_{g0} = 0.7$ [*m / s*], Φ =

0.363 and h = 1500 [W/m^2K], to obtain 2.05 [V] electrical potential, 21 [W] of electrical power and an overall efficiency of process η = 5.64%.

Acknowledgements - The support of CONICYT – Chile under FONDECYT Project 1131156, and of the Aeronautical Polytechnic Academy, FACH, Chile, is gratefully acknowledged.

REFERENCES

[1] Mößbauer S., Pickenäcker O., Pickenäcker K., Trimis D., Application of the porous burner technology in energy and heat engineering, in: *Fifth International Conference on Technologies and Combustion for a Clean Environment (Clean Air V), Lisbon, Portugal*, Vol. 1, Lecture 20.2, 1999, pp. 519–523.

[2] Bubnovich Valeri I., Toledo Mario, Experimental study of a diluted methane–air mixture combustion under filtration in a packed bed, *IASME Trans*., Vol. 1, No 3, 2004, pp. 574–577.

[3] Mathis Jr. W.M., Ellzey J.L., Flame stabilization operating range and emissions for a methane/air porous burner, *Combust. Sci. Technol.*, Vol. 175, 2003, pp. 825–839.

[4] Trimis D., Durst F., Combustion in a porous medium-advances and applications, *Combust. Sci. Technol.*, Vol. 121, 1997, pp. 153–168.

[5] Toledo Mario, Bubnovich Valeri, Saveliev Alexei, Kennedy Lawrence, Filtration combustion of methane, ethane, and propane mixtures with air, *WSEAS Trans. Heat Mass Transfer*, Vol. 1, No. 3, 2006, pp. 283–292.

[6] Dobrego K.V., Gnesdilov N.N., Kozlov I.M., Bubnovich V.I., Gonzalez H.A., Numerical investigation of the new regenerator–recuperator scheme of VOC oxidizer, *Int. J. Heat Mass Transfer*, Vol. 48, 2005, pp. 4695–4703.

[7] Moraga Nelson O., Rosas César E., Bubnovich Valeri I., Tobar José R., Unsteady fluid mechanics and heat transfer study in a double-tube air–combustor heat exchanger with porous medium, *Int. J. Heat Mass Transfer*, Vol. 52, 2009, pp. 3353– 3363.

[8] Babkin V.S., Filtrational combustion of gases. Present state of affairs and prospects, *Pure Appl. Chem.*, Vol. 65, No. 2, 1993.pp. 335–344.

[9] Howell J.R., Hall M.J., Ellzey J.L., Combustion of hydrocarbon fuel within porous inert media, *Prog. Energy Combust. Sci.*, Vol. 22, 1996, pp. 121–145.

[10] Bubnovich V., Henríquez L., Gnesdilov N., Numerical study of the effect of the diameter of alumina balls on flame stabilization in a porous media burner, *Numer. Heat Transfer A, Appl.*,Vol. 52, No. 3, 2007, pp. 275–295.

[11] Bubnovich V., Toledo M., Henríquez L., Rosas C., Romero J., Flame stabilization between two beds of alumina balls in a porous burner, *Appl. Therm. Eng.*, Vol. 30, 2010, pp. 92–95.

[12] Babkin V.S., Korzhavin A.A., Bunev V.A., Propagation of premixed gaseous explosion flames in porous media, *Combust. Flame*, Vol. 87, 1991, pp. 182–190.

[13] Brenner G., Pickenäcker K., Pickenäcker O., Trimis D., Wawrzinek K., Weber T., Numerical and experimental investigation of matrix-stabilized methane/air combustion in porous inert media, *Combust. Flame*, Vol. 123, 2000, pp 201–213.

[14] Bouma P.H., De Goey L.P.H., Premixed combustion on ceramic foam burners, *Combust. Flame*, Vol. 119, 1999, pp.133–143.

[15] Hoffmann J.G., Echigo R., Yoshida H., Tada S., Experimental study on combustion in porous media with a reciprocating flow system, *Combust. Flame*, Vol. 111, 1997, pp. 32–46.

[16] Contarin F., Saveliev A.V., Fridman A.A., Kennedy L.A., A reciprocal flow filtration combustor with embedded heat exchangers: numerical study, *Int. J. Heat Mass Transfer*, Vol. 46, 2003, pp. 949–961.

[17] Bubnovich Valeri, Henriquez Luis, Diaz, Catalina Avila Emilio, Stabilization operation region for a reciprocal flor burner, recent advances in applied and theoretical mechanics, in: *Proceedings of the Fifth WSEAS International Conference on Applied and Theoretical Mechanics (Mechanics'09), Puerto De La Cruz, Tenerife, Canary Islands, Spain, December 14–16*, 2009, pp. 114–119.

[18] Mao-Zhao Xie, Jun-Rui Shi, Yang-Bo Deng, Hong Liu, Lei Zhou, You-Ning Xu, Experimental and numerical investigation on performance of porous medium burner with reciprocating flow, *Fuel*, Vol. 88, 2009, pp. 206–213.

[19] Contarin F., Barcellos W.M., Saveliev A.V., Kennedy L.A., Energy extraction from a porous media reciprocal flow burner with embedded heat exchangers, *Heat Mass Transfer*, Vol. 127, No. 2, 2005, pp.123–130.

[20] Zhdanok S.A., Dobrego K.V., Foutko S.I., Flame localization inside axisymmetric cylindrical and spherical porous media burners, *Int. J. Heat Mass Transfer*, Vol. 41, 1998, pp. 3647–3655.

[21] Zhdanok S., Kennedy L.A., Koester G., Superadiabatic combustion of methane air mixtures under filtration in a packed bed, *Combust. Flame*, Vol. 100, 1995, pp. 221– 231.

[22] Hanamura K., Echigo R., Superadiabatic combustion in a porous medium, *Int. J. Heat Mass Transfer*, Vol. 36, No. 13, 1993, pp. 3201–3209.

[23] Foutko Serguei I., Shabunya Stanislav I., Zhdanok Serguei A., Superadiabatic combustion wave in a diluted methane-air mixture under filtration in a packed bed, *Twenty-Sixth Symposium (International) on Combustion/The Combustion Institute, Pittsburgh*, 1996, pp. 222-227.

[24] Henneke Michael R., Ellzey Janet L., Modeling of Filtration Combustion in a Packed Bed, *Combustion and Flame*, No. 117, 1999, pp. 832-840.

[25] Min G. and Rowe D.M., Ring-structured thermoelectric module, *Semiconductor Science and Technology*, Vol. 22, No 8, 2007, pp. 365-371.